Hindawi
Journal of Nanomaterials
Volume 2022, Article ID 3528664, 10 pages
https://doi.org/10.1155/2022/3528664

Research Article

Properties and Modification of Bismuth-Layered Structure Ferroelectric Materials and Application in Sports

Guorong Jiang

School of Sports, Jiujiang University, Jiujiang, 332005 Jiangxi, China

Correspondence should be addressed to Guorong Jiang; 2021001548@poers.edu.pl

Received 8 March 2022; Revised 18 June 2022; Accepted 7 July 2022; Published 24 August 2022

Academic Editor: Awais Ahmed

Copyright © 2022 Guorong Jiang. This is an open access article distributed under the Creative Commons Attribution License, which permits unrestricted use, distribution, and reproduction in any medium, provided the original work is properly cited.

Bismuth-layered oxides are a very important class of ferroelectric materials. Due to their special structure, they have outstanding features in many aspects, such as high Curie temperature, large spontaneous polarization, polarization stability to temperature, high voltage resistance, low dielectric loss, and excellence. Due to its antifatigue properties, the system is very suitable for applications in nonvolatile random access memory and high-temperature sensors. The purpose of this paper is to study the application of the performance and modification of bismuth-layered ferroelectric materials in sports scientific research. Proposed the combination of new materials and sports scientific research projects. This article uses sample analysis and (the comparative experiment method is a method to compare the experimental group and the control group to illustrate the superiority of the experiment) comparative experiment methods, sets up an experimental group and a control group, summarizes the algorithm rules through the study of the microscopic properties of nanomaterials, and designs a numerical simulation program. The experimental results in this article show that after receiving hyperbaric oxygen recovery in the first week, the heart rate of the experimental group subjects has a significant change, which is significantly lower than the initial value ($p < 0.05$), from 58.0 to 53.0, The higher pressure oxygen had a very significant drop before recovery, from 62.9 to 53.0. In the second week and the third week, the heart rate index decreased significantly after 1 hour of hyperbaric oxygen recovery ($p < 0.01$), from 54.3 to 49.3 and 56.1 to 52.4, respectively. After the fourth week of intensity training, the heart rate increased significantly from the initial value ($p < 0.05$), from 49.6 to 55.2. After 1 hour of hyperbaric oxygen recovery, there was a significant decrease compared with before the hyperbaric oxygen recovery ($p < 0.05$), dropped from 55.2 to 53.1. Illustrate the success of the experimental results. It also completed the subject of interaction and combination of the performance and modification of bismuth-layered ferroelectric materials in sports scientific research.

1. Introduction

In a certain temperature, the ferroelectric material exhibits the characteristics of spontaneous polarization when there is no external electric field, and its polarization may have multiple directions. When an electric field is applied, the polarization direction changes with the change of the electric field. Generally, after the temperature exceeds a certain value, the spontaneous polarization of the ferroelectric material will disappear, and the ferroelectric material will become paraelectric. The transition between ferroelectricity and paraelectricity is called ferroelectric phase transition. Many physical properties of crystals at this temperature are different from usual, and the temperature of this transition is the Curie point of ferroelectrics. In addition to spontaneous polarization, the hysteresis loop is also an important way to observe whether a crystal is a ferroelectric. Research shows that the polarization intensity and direction of the crystal will exhibit a dielectric characteristic different from ordinary materials with the applied electric field. Ferroelectric materials are special electrolytes and have been extensively studied. It has a variety of polarization modes, which have different effects at different frequencies, so that the dielectric spectrum of different materials is very different. From the microscopic mechanism, it can be attributed to two different types: (1) displacement type and (2) order and disorder type. Frequency-tunable materials have potential applications in the fields of frequency selection,

absorption, imaging, and biology. Certain elements are sensitive to temperature changes. Doping these elements in ferroelectric materials can affect its dielectric properties. Ferroelectric materials are widely used in subject interaction due to their unique properties.

Multiferroic materials with ferromagnetism and ferroelectricity are mainly concentrated in transition metal (rare earth element) oxides, mainly due to their complex electronic structures and competing interactions. These competitions include charge, spin, orbital, and lattice degrees of freedom, which are more easily regulated by external means (such as electric field, magnetic field, and stress). At the same time, multiferrocity requires that the d or f orbitals of transition metals or rare earth elements must be partially filled with local electrons, and through exchange interactions between local moments, magnetic order (time reversal broken) is caused. On the other hand, for ferroelectric materials, in order to induce spontaneous polarization (spatial inversion broken), empty d orbitals are required. Few systems can meet these two requirements at the same time, so there are very few multi-iron materials in nature. According to the microscopic sources of different iron-containing properties, multicore materials can be divided into different types, and the magnetic properties of materials can generally be divided into paramagnetic, antiferromagnetic, and ferromagnetic. When the magnet is lower than the Curie temperature, it is ferromagnetic; when it is higher than the Curie temperature, it is macroscopically paramagnetic. Adjacent magnetic atoms have different magnetic coupling results, leading to different magnetic orientations, leading to different magnetic step settings. In the rectangular perovskite system, ferromagnetism (FM), the magnetic orientation of all its atoms is the same. For diamagnetism, there are four different magnetic orientations, namely, A-type diamagnetism (A-AFM): the orientation of the magnetic order of the atoms in the plane is the same, and the magnetic order of the atoms in the plane is opposite. Diamagnetic C-type (C-AFM): the magnetic order of atoms in the plane is diamagnetic order, and the magnetic order of atoms in the plane is diamagnetic. The magnetic order between the outer atoms is the same. Antimagnetic G (G-AFM): the magnetic sequence of the nearest neighbor is opposite. E-AFM: the magnetic orientation of diamagnetism is along the AC plane, and individuals with the same magnetic orientation are saw-shaped.

From 1935 to 1938, Basheer et al. discovered that the simple structure of potassium dihydrogen phosphate (KDP) and many of its isomorphic crystals are also piezoelectric, and all have high room temperature electromechanical coupling coefficients. But they did not propose the concept of piezoelectric effect [1]. The piezoelectric effect was first discovered in quartz crystal by Nie et al. in 1880. Its discovery led to the rapid development of piezoelectric devices and piezoelectric materials. However, due to time constraints, their research did not further analyze other media and materials related to the piezoelectric effect [2]. In 1954, Ketwong et al. discovered the quasihomomorphic phase boundary (MPB) of Pb $(Zr,Ti)O_3$(PZT) system solid solution. The ferroelectric near MPB has excellent dielectric and piezoelectric properties, and it is close to $BaTiO_3$ ceramics. The high electromechanical coupling coefficient has made piezoelectric materials widely used, but their research stopped here, and the ferroelectricity of subsequent perovskite structure compounds was not found [3].

The innovations of this paper are as follows: (1) in the research content, the macroscopic research method, the transfer matrix method, is selected to study the microstructure characteristics of the crystal. The characteristic matrix is used to express its interaction with electromagnetic waves. (2) The $Bi_4Ti_3O_{12}$ crystal was selected as the bismuth-layered ferroelectric material in this article. The crystal has stable properties, relatively good ferroelectricity, and convenient preparation. (3) The research and introduction of the ferroelectric polarization value have been carried out, making the concept of perfecting the text clear.

The new materials adopted in this article are combined with traditional sports scientific research to meet the needs of subject interaction.

2. Performance and Modification of Bismuth-Layered Structure Ferroelectric Materials and Application Methods in Sports Scientific

2.1. Ferroelectricity. The ferroelectric system is a substance that has spontaneous polarization after transitioning from a high-temperature phase to a low-temperature phase, and its polarization direction can be reversed by an external electric field [4]. Many properties of ferroelectric systems are similar to ferromagnets. For example, electric polarization (P) corresponds to magnetization (M), electric field (E) corresponds to magnetic field (H), and electric displacement (D) corresponds to magnetic flux density (B) [5]. At the same time, ferroelectric materials can form domains, and their polarization and electric displacement exhibit electric hysteresis loop behavior in the applied electric field. Therefore, ferroelectric materials can be used for data storage. Research has found that ferroelectric materials can also be used as capacitors, because the concentration of charge density in ferroelectric materials will cause them to have a high dielectric constant [6].

The early work of ferroelectric materials mainly focused on Rochelle salt, $KNa(C_4H_4O_6)\cdot 4H_2O$. Although the research of Rochelle's salt has established many basic properties of ferroelectric materials, the complex structure and the large number of atoms in each cell make it difficult to give a microscopic theory to clarify ferroelectricity from an experimental point of view [7]. At present, the widely studied ferroelectric system is the perovskite structure oxide ABO3. The ideal perovskite structure is characterized by a cation (B) with a small particle radius, in the center composed of an anionic oxygen octahedron, and the particle radius. The larger cation (A) is at the apex of the primitive cell [8]. The relatively simple structure of perovskite allows researchers to study its ferroelectric properties in detail and have a deeper understanding of the basic principles of ferroelectricity [9].

Table 1 is an introduction to 32 crystallographic point groups.

Table 1: 32 crystallographic point groups.

T	Th	O	Td	Oh		
C4	S4	C4h	D4	C4v	D2d	D4h
D2	C2v	D2h				
C2	Cs	C2h				
C1	Ci					
C3	S6	D3	C3v	D3d		
C6	C3h	C6h	D6	C6v	D3h	D6h

Symmetry determines whether the system is ferroelectric. Among the 32 crystallographic point groups, 11 crystallographic point groups have a center of symmetry (centrosymmetric); that is, they do not have ferroelectricity; in the remaining 21 point groups, the O point group does not have ferroelectricity. The remaining 20 all show piezoelectric effect, but only 10 point groups have its specific polarity direction [10].

2.2. Preparation Technology. The traditional solid-phase melting process is used to manufacture bismuth-coated ceramic powder. The uniformity of the powder is low, and the melting temperature is high [11]. It is difficult to obtain ceramic samples with high density and excellent performance [12]. In recent years, some liquid chemical methods, such as sol-gel method, hydrothermal synthesis method, and other powder preparation methods, have gradually attracted the attention of scientific researchers [13]. The use of liquid chemical methods to manufacture ceramic powder can achieve molecular-level mixing between the various components of the material [14], with high product purity, large powder specific surface area, and high ceramic fusion temperature, which can also be reduced to a certain extent. The sol-gel method was used to prepare ceramic powder $(K_{0.16}Na_{0.84})_{0.5}Bi_{4.5}Ti_4O_{15}$ (KNBT) [15], and the phase structure and electrical properties were studied. Studies have found that when the composition temperature is 500°C, single-phase KNBT ceramic powder can be formed, and the Curie temperature of the ceramic sample is 659°C [16], which is higher than the Curie temperature of KNBT ceramic prepared by traditional methods. The ferroelectric ceramics of the $SrBi_4$-$xCexTi_4O_{15}$ system can also be successfully prepared by the sol-gel method. The study found that all ceramic samples formed a typical phase structure with a bismuth layer, and the Curie temperature of the samples was above 500°C [17]. In short, the use of different powder preparation techniques will definitely have different effects on the structure and performance of ceramic samples [18]. This liquid chemical method can prepare ceramic powder with uniform particle size and large specific surface area. However, the cost of raw materials used in this type of process is high, the experimental process is complicated, and the organic solvent used in the reaction process is toxic and difficult to achieve. Batches of lead-free bismuth piezoelectric ceramics have a wide range of applications in industrial production and can be used in the research of this article [19].

Lead-free dual-structure piezoelectric materials are widely used in the research of ferroelectric thin films and devices due to their fatigue resistance and high-temperature Curie characteristics [20]. However, due to the limitation of its own structure, it is difficult to effectively improve the two-level performance of ceramics, ferroelectric properties, and piezoelectric properties [21, 22]. The physical and chemical properties of materials are determined by the structure of the material, and the structure of the material is related to the composition of the material. Therefore, replacing the composition and structure of ceramic crystals with doping is an effective measure to improve the electrical properties of bismuth ceramics [23, 24]. This type of method has low preparation cost and simple process and is suitable for a wide range of applications [25]. At present, the doping modification methods of bismuth lead-free piezoelectric ceramics mainly include A-site substitution, B-site substitution, and additive modification [26].

2.3. Transfer Matrix Method. The matrix transmission method (TMM) is a method that combines the knowledge of Maxwell's equations (It is a set of partial differential equations established by British physicist James Clark Maxwell in the 19th century to describe the relationship between electric field, magnetic field, charge density, and current density.) and optical matrices to calculate the transmission and reflection propagation of electromagnetic waves in multiple layers of different media structures. The propagation of electromagnetic waves in the intermediate layer is considered to be the superposition of incident electromagnetic waves and reflected electromagnetic waves. The tangent continuous state of the electromagnetic field is satisfied at the limit of each intermediate layer, and its interaction with electromagnetic waves can be represented by a characteristic matrix. Assuming that the field vectors on both sides of the dielectric layer are EI and HI and EII and HII, the relationship between them can be linked by the characteristic matrix:

$$\begin{bmatrix} E_1 \\ H_1 \end{bmatrix} = M \begin{bmatrix} E_{11} \\ H_{11} \end{bmatrix}. \tag{1}$$

For interface I,

$$\left\{ \begin{array}{c} E_1 = E_{i1} + E_{r1} = E_{t1} + E'_{r2} \\ H_1 = H_{i1} \cos\theta_{i1} - H_{r1} \cos\theta_{i1} \end{array} \right\}. \tag{2}$$

In the same way, in interface II,

$$\left\{ \begin{array}{c} E_{\mathrm{II}} = E_{i2} + E_{r2} = E_{r2} + E'_{r3} \\ H_{\mathrm{II}} = H_{i2} \cos\theta_{i2} - H_{r2} \cos\theta_{i2} \end{array} \right\}. \tag{3}$$

The thickness of the medium nb is b (that is, the distance between the interfaces I and II), and the formula of

the transmission field E_{t1} on the interface I and the incident field E_{i2} of the interface II is shown in

$$\begin{cases} E_{t1} = E_{t10}e^{-i(k_x x + k_z z)}\Big|_{z=0}, \\ E_{t2} = E_{t10}e^{-i(k_x x + k_z z)}\Big|_{z=b} = E_{t1}e^{i\delta_b}. \end{cases} \tag{4}$$

The phase difference when the electromagnetic plane wave crosses the two interfaces perpendicularly is

$$\delta_b = -k_z h_b = -\frac{\omega}{c} n_b b \cos\theta_b. \tag{5}$$

The same goes for

$$E'_{r2} = E_{r2}e^{i\delta_b}. \tag{6}$$

Organize to get

$$\begin{cases} E_1 = \cos\delta_b E_{\text{II}} - \dfrac{1}{\eta_b}\sin\delta_b H_{\text{II}}, \\ H_1 = -i\eta_b \sin\delta_b E_{\text{II}} + \cos\delta_b H_{\text{II}}, \end{cases} \tag{7}$$

where

$$\eta_b = \sqrt{\frac{\varepsilon_0}{\mu_0}}\sqrt{\frac{\varepsilon_r}{\mu_0}}\cos\theta_b. \tag{8}$$

In matrix form, there are

$$\begin{bmatrix} E_1 \\ H_1 \end{bmatrix} = \begin{bmatrix} \cos\delta_b & -\dfrac{1}{\eta_b}\sin\delta_b \\ -i\eta_b \sin\delta_b & \cos\delta_b \end{bmatrix} \begin{bmatrix} E_{\text{II}} \\ H_{\text{II}} \end{bmatrix}. \tag{9}$$

The characteristic matrix of any dielectric layer j is

$$M_j = \begin{bmatrix} \cos\delta_j & -\dfrac{i}{\eta_j}\sin\delta_j \\ -i\eta_j \sin\delta_j & \cos\delta_j \end{bmatrix}. \tag{10}$$

For the case in TTE mode, where

$$\begin{cases} \delta_j = -\dfrac{\omega}{c} n_j h_j \cos\theta_j, \\ n_j = \sqrt{\dfrac{\varsigma_0}{\mu_0}}\sqrt{\dfrac{\mu_j}{\varepsilon_j}}\cos\theta_j. \end{cases} \tag{11}$$

In the case of TM mode, the other formulas are the same, but the key variables are replaced:

$$n_j = \sqrt{\frac{\mu_0}{\varepsilon_0}}\sqrt{\frac{\mu_j}{\varepsilon_j}}\cos\theta_j. \tag{12}$$

For multilayer media, it can be applied layer by layer, then:

$$\begin{bmatrix} E_1 \\ H_1 \end{bmatrix} = M_1 M_2 \cdots M_{N-1} M_N \begin{bmatrix} E_{N+1} \\ H_{N+1} \end{bmatrix} = \begin{bmatrix} A & B \\ C & D \end{bmatrix} \begin{bmatrix} E_{N+1} \\ H_{N+1} \end{bmatrix}. \tag{13}$$

The transmittance T, reflectance R, and absorptance A are

$$\begin{cases} T = |t|^2, \\ R = |r|^2, \\ A = 1 - T - R. \end{cases} \tag{14}$$

Among them,

$$\begin{cases} \delta_a = -\dfrac{\omega}{c} n_a a \cos\theta_a, \\ \delta_b = -\dfrac{\omega}{c} n_b b \cos\theta_b, \\ \eta_a = \sqrt{\dfrac{\varepsilon_0}{\mu_0}}\sqrt{\dfrac{\varepsilon_0}{\mu_0}}\cos\theta_a, \\ \eta_b = \sqrt{\dfrac{\varepsilon_0}{\mu_0}}\sqrt{\dfrac{\varepsilon_0}{\mu_0}}\cos\theta_b. \end{cases} \tag{15}$$

In summary, the introduction of the transmission matrix method is complete, and the experiment is ready to begin.

3. Performance and Modification of Bismuth-Layered Structure Ferroelectric Materials and Application Experiments in Sports Scientific

3.1. Preparation and Application of $Bi_4Ti_3O_{12}$ Powder. $Bi_4Ti_3O_{12}$ material has a low forbidden band width and photocatalytic activity, and its absorbable spectral range can be extended to the visible light range through the method of nanomaterialization or doping modification of the material. This plays an important role in improving the utilization of sunlight. In addition, it is a typical ferroelectric material with good ferroelectric and piezoelectric properties. In this chapter, $Bi_4Ti_3O_{12}$ powder is prepared by hydrothermal method, and the role of hydrothermal temperature in the preparation process is discussed. The key work of this chapter is to apply ultrasound and light to $Bi_4Ti_3O_{12}$ powder at the same time. It is expected that ultrasound can be used to activate the piezoelectric properties of bismuth titanate, to achieve polarization of bismuth titanate powder, and to improve its photocatalytic efficiency.

In this paper, $Bi_4Ti_3O_{12}$ powder is prepared by hydrothermal method. The preparation process can be divided into three steps: preparation of hydrothermal reaction precursor, hydrothermal reaction, and heat treatment of hydrothermal product. Among them, bismuth nitrate is used as

Table 2: The main drugs needed for the experiment.

Reagent name	Specification	Manufacturer
Bismuth nitrate	Analytically pure	Sinopharm
Tetrabutyl titanate	Analytically pure	Sinopharm
Ethylene glycol monomethyl ether	Analytically pure	Sinopharm
Glacial acetic acid	Analytically pure	Coron
Acetylacetone	Analytically pure	Sinopharm
Disodium ethylenediaminetetraacetate	Analytically pure	Sinopharm
Tert-butanol	Analytically pure	Sinopharm

Table 3: Basic situation of the athlete group.

Group	Number	Average age	Average height	Average weight	Main item		Sport level	
					5/10 km	Marathon	International master	Master
Athlete	130	23.1	169.29	55.53	91	31	43	79
Male athlete	65	24.27	174.98	61.48	46	15	11	50
Female athlete	65	20.84	163.53	49.48	45	16	32	29

Table 4: Basic situation of the control group.

Group	Number	Average age	Average height	Average weight
Control	130	21.53	173.4	63.99
Male	65	20.29	174.95	69.23
Female	65	19.96	163.03	56.97

the titanium source, tetrabutyl titanate is used as the bismuth source, and 3 mol/L NaOH solution is used as the mineralizer for the hydrothermal reaction. First, 30 mL of glacial acetic acid and 30 mL of ethylene glycol methyl ether are mixed, and then, 9.7 g of bismuth nitrate is added to form solution A; then, 5.10 g of tetrabutyl titanate is dissolved in 20 mL of ethylene glycol methyl ether to form solution B. Finally, solution B was slowly added to solution A, and an appropriate amount of ethylene glycol methyl ether was added to prepare a 0.05 M bismuth titanate sol. After drying the sol, a dry gel is obtained, and the dry gel is ground and dissolved in a mineralizer to prepare a hydrothermal reaction precursor. After the preparation of the hydrothermal precursor is completed, the hydrothermal precursor solution is put into the reaction kettle and put into the oven for hydrothermal reaction. Through literature research and consideration of experimental safety, three hydrothermal temperature points of 160°C, 180°C, and 200°C that do not exceed 200°C are selected for the experiment, and the holding time is 24 h.

The main experimental drugs are shown in Table 2.

3.2. Objects of Experiments. The subjects of this study are divided into the excellent long-distance runner group (case) and the general population control group (control group).

The basic situation of the outstanding long-distance runner group is shown in Table 3.

The athletes and ordinary personnel in this experiment were taken from two classes in a major physical education department and a certain electrical engineering department with the same basic situation, each with 130 students as samples.

The basic situation of the control group is shown in Table 4.

3.3. Test Instrument and Test Index. The equipment used in the exercise capacity test is hyperbaric oxygen equipment, 0.035 MPa, and the maximum working load is 0.05 MPa.

In the HRV test, the omega wave test and analysis system are used to collect signals, and Excel is used for index calculation. Use the SPSS24.0 software statistical package to perform statistical processing on the data. $p < 0.05$ indicates a significant difference.

4. Application of the Performance and Modification of Bismuth-Layered Ferroelectric Materials in Sports Scientific

4.1. Influence of $Bi_4Ti_3O_{12}$ on the Quiet Heart Rate of Middle and Long Distance Runners. Figure 1 shows the initial value of heart rate in the experimental group during the experimental period, before the recovery of hyperbaric oxygen, and the change of resting heart rate after 1 hour of recovery.

After receiving hyperbaric oxygen recovery in the first week, the heart rate of subjects in the experimental group changed significantly from the initial value ($p < 0.05$), from 58.0 to 53.0, before the higher oxygen pressure was restored. There has been a very significant drop, from 62.9 to 53.0. In the second week and the third week, the heart rate index decreased significantly after 1 hour of hyperbaric oxygen

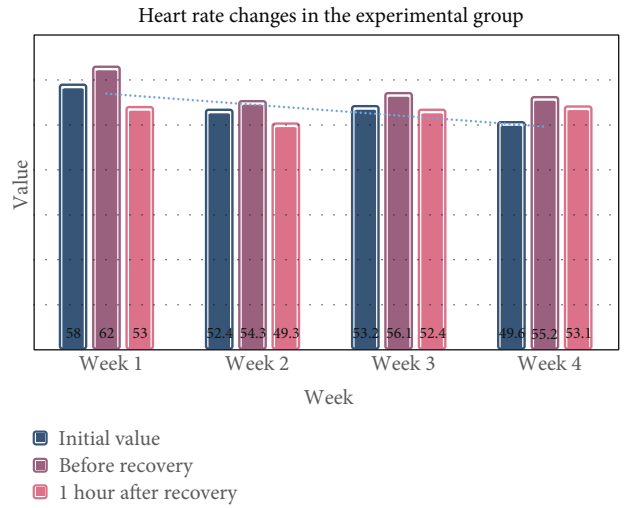

Figure 1: Heart rate changes in the experimental group.

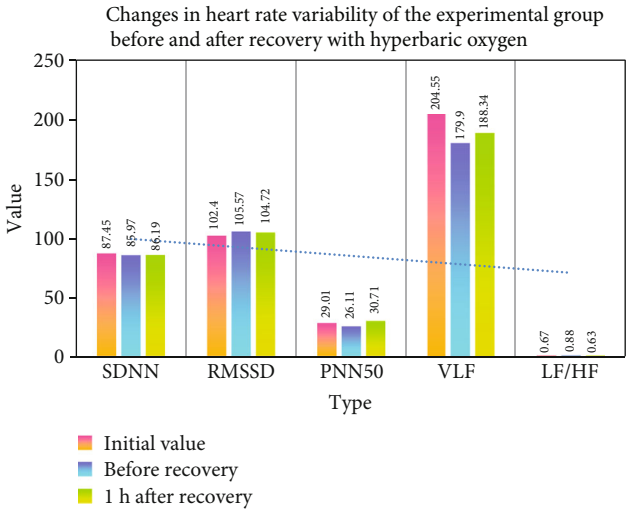

Figure 2: Changes in heart rate variability of the experimental group before and after recovery with hyperbaric oxygen in the first week.

recovery ($p < 0.01$), from 54.3 to 49.3 and 56.1 to 52.4, respectively. After the fourth week of intensity training, the heart rate increased significantly from the initial value ($p < 0.05$), from 49.6 to 55.2. After 1 hour of hyperbaric oxygen recovery, there was a significant decrease compared with before the hyperbaric oxygen recovery ($p < 0.05$), dropped from 55.2 to 53.1.

The changes in heart rate variability of the experimental group before and after recovery using hyperbaric oxygen in the first week are shown in Figure 2.

It can be seen that there is no significant change in the time domain indicators of heart rate variability.

The initial value of the experimental group in the second week, before the recovery of hyperbaric oxygen, and the change of heart rate variability index after the recovery of hyperbaric oxygen for 1 hour are shown in Figure 3.

In the second week, the time domain indicators SDNN, RMSSD, and PNN50 of the experimental group showed a

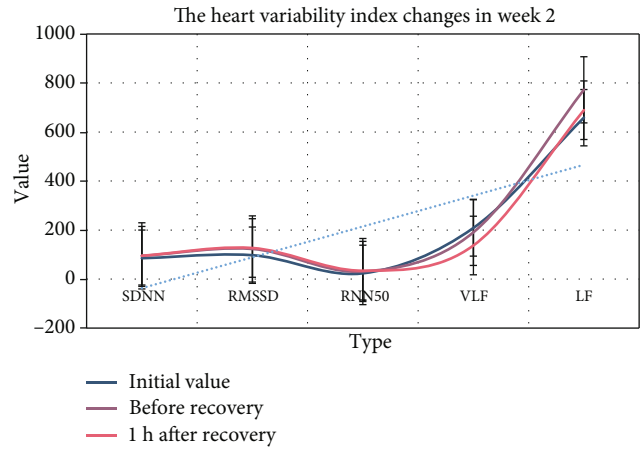

Figure 3: The initial value of the experimental group in the second week, before the recovery of hyperbaric oxygen, and the change of heart rate variability index after 1 hour of hyperbaric oxygen recovery.

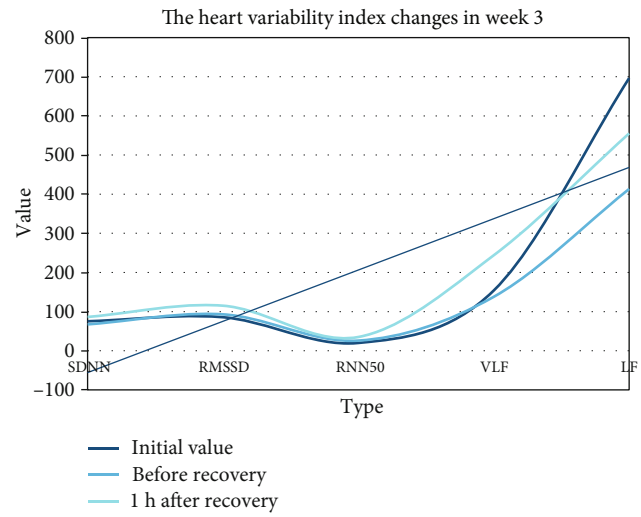

Figure 4: The initial value of the experimental group in the third week, before the recovery of hyperbaric oxygen, and the change of heart rate variability index after 1 hour of hyperbaric oxygen recovery.

slight upward trend from the initial value before the hyperbaric oxygen recovery and 1 h after receiving the hyperbaric oxygen recovery, but there was no significant difference. One hour after the recovery of hyperbaric oxygen, the change before the recovery of higher pressure oxygen was not obvious. The VLF in the frequency domain indicators of the subjects decreased sequentially, but there was no significant difference. The change of HF and LF is not obvious.

The initial value of the experimental group in the third week, before the recovery of hyperbaric oxygen, and the change of heart rate variability index after the recovery of hyperbaric oxygen for 1 hour are shown in Figure 4.

It can be seen from the above table that in the time domain index, the initial value of PNN50, the value before hyperbaric oxygen recovery, and the value after hyperbaric

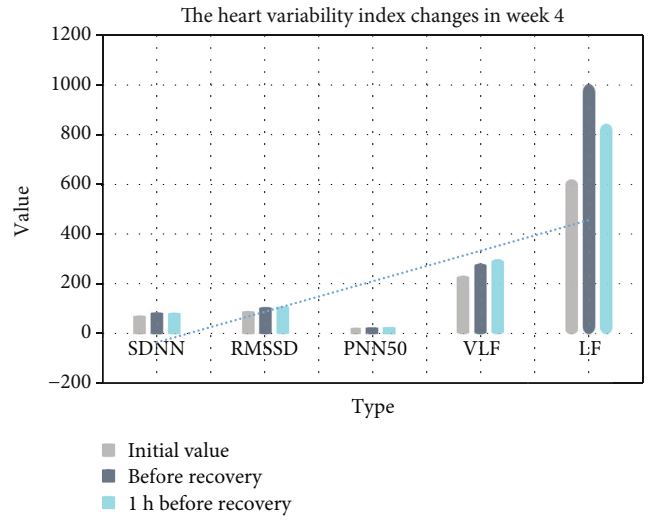

Figure 5: The heart variability index changes in week 4.

Table 5: The experimental group did not apply hyperbaric oxygen for two weeks during the observation period to restore the changes in heart rate variability.

Heart rate variability index	First week of observation period	Second week of observation period
SDNN	85.12	70.80
RMSSD	85.65	81.54
PNN50	22.04	19.99
VLF	305.77	209.38
HF	165.13	1095.35
LF	817.80	537.79
HF/LF	1.17	1.35

Table 6: The calculated ferroelectric polarization of ABX_3 perovskite halide compounds.

System	Px	Py	Pz	Ptot
$MASncl_3$	-8.68	0.94	9.58	12.96
$MASnBr_3$	8.03	8.67	-15.08	19.16
$MASnI_3$	-3.78	0.00	15.63	16.08
$MAPbCl_3$	4.01	4.59	-11.48	13.00
$MAPbBr_3$	-3.38	-3.60	11.70	12.70
$MAPbI_3$	2.68	2.68	13.52	14.03
$FASnC_{l3}$	3.30	-4.64	-13.85	14.98

Px refers to the microscopic component of the material on the x-axis.

oxygen recovery 1 h showed a sequential upward trend, and the initial value after 1 h hyperbaric oxygen recovery appeared compared with the initial value. There was a significant increase ($p < 0.05$), from 19.93 to 35.12, and the RMSSD value also showed an upward trend, but there was no significant change. In the frequency domain indicators, both VLF and LF showed a downward trend and then an upward trend. HF showed a sequential upward trend, but there was no significant difference. LF/HF showed a downward trend, but it did not appear significant.

The initial value of the experimental group in the fourth week, before the recovery of hyperbaric oxygen, and the change of heart rate variability index after the recovery of hyperbaric oxygen for 1 hour are shown in Figure 5:

In the time domain index, the value of RMSSD in the experimental group was higher after 1 hour of hyperbaric oxygen recovery, and there was a significant increase ($p < 0.05$), from 108.91 to 111.70, while the changes in SDNN and PNN50 were not very obvious and not significant. In the frequency domain parameters of the subjects, HF increased significantly ($p < 0.05$) from 1354 to 1683 after receiving hyperbaric oxygen treatment for 1 hour than before hyperbaric oxygen recovery. LF also increased from the initial value before hyperbaric oxygen recovery. After

Table 7: Estimated Rashba parameters for organohalide perovskites.

	Er		Ke		aR	
	VB	CB	VB	CB	VB	CB
$MASncl_3$	7.19	182.38	0.04	0.16	0.37	2.28
$MASnBr_3$	18.87	143.52	0.03	0.09	1.28	3.29
$MASnI_3$	28.44	99.45	0.04	0.06	1.56	3.12
$MAPbCl_3$	7.81	113.41	0.02	0.09	0.65	2.56
$MAPbBr_3$	25.88	120.30	0.04	0.08	1.28	3.01
$MAPbI_3$	72.62	136.01	0.08	0.08	1.86	3.50
$FASnC_{13}$	8.62	142.97	0.0.3	0.13	0.49	2.18

Table 8: Crystal information and refinement conditions of $Bi_4Ti_3O_{12}$ at room temperature.

Atom	Site	X	y	z	100Uiso/A2	Occupancy
Bil	4a	0.25	0.7726 (14)	0	0.95	0.505
Lal	4a	0.25	0.7726 (14)	0	0.95	0.495
Bi2	8b	0.244 (9)	0.7266 (9)	0.21672 (8)	1.05	0.757
La2	8b	0.244 (9)	0.7266 (9)	0.21672 (8)	1.05	0.243
Bi3	8b	0.248 (8)	0.7804 (8)	0.10695 (10)	1.09	0.952
La3	8b	0.248 (8)	0.7804 (8)	0.10695 (10)	1.09	0.018
Ti1	8b	0.252 (19)	0.257 (4)	0.0586 (4)	0.19	0.75

receiving treatment for 1 hour, the trend of AIDS decreased, but there was no significant change.

In the fifth and sixth weeks, the experimental group stopped hyperbaric oxygen during the observation period and resumed the initial value of the heart rate on the week, as shown in Table 5.

The subjects' various time-domain indicators have declined, but there is no significant difference, and there is little change. The values of VLF and LF have a downward trend, HF does not change significantly, and LF/HF rises, but there is no significant difference. SDNN is an indicator of heart rate variability; generally, it is greater than 100.

4.2. Iron Polarization Value. The ferroelectric polarization value is zero for the antiferroelectric structure ($\lambda = 0$), and the subsequent trend shows that a nonmonotonic line increases with λ. The nonmonotonic behavior as a lambda function is common in the case of organic-inorganic hybrid compounds. At the same time, the components of the total ferroelectric polarization vector and the modulus of the vector are calculated by the first principles, as shown in Table 6.

The estimated Rashba coefficient in organic halide perovskite is shown in Table 7.

4.3. $Bi_4Ti_3O_{12}$ Microstructure and Ferroelectric Properties. Table 8 is the crystal information and refinement conditions of $Bi_4Ti_3O_{12}$ at room temperature.

It can be seen from the table that the contribution of the total spontaneous polarization of $Bi_4Ti_3O_{12}$ is better, and the ferroelectricity is increased. It shows that the phase reversal does come from signal polarization reversal and ferroelectric behavior, which is higher than 0.26 nm in OPP mode.

5. Conclusions

The experimental results show that the performance and modification research of the bismuth-layered ferroelectric material proposed in this paper is applied in sports scientific research. Compared with the current traditional sports scientific research, due to the use of a new type of bismuth-layered ferroelectric material, as a result, the effect of scientific research is better. After athletes use the material for long-distance running assistance, all data and performance have increased significantly. The observation effect is better, the data collection is more accurate, and it is more convenient for sports-assisted scientific research personnel and researchers to judge and test. In this paper, sample collection method, comparison experiment method, and transmission matrix method are used to design a method to calculate the transmittance and reflectance of electromagnetic wave propagation in multilayer different media structures by combining the knowledge of Maxwell's equation and matrix optics. And the changes in heart rate variability before and after 4-week recovery with hyperbaric oxygen in the control and experimental groups were also tested. The experimental results showed that after receiving hyperbaric oxygen recovery in the first week, the heart rate of the experimental group subjects changed significantly, which was significantly lower than the initial value ($p < 0.05$), from 58.0 to 53.0. There was a very significant drop before hyperbaric oxygen recovery, from 62.9 to 53.0. In the second week and the third week, the heart rate index decreased significantly after 1 hour of hyperbaric oxygen recovery ($p < 0.01$), from 54.3 to 49.3 and 56.1 to 52.4, respectively. After the fourth week of intensity training, the heart rate increased significantly from the initial value ($p < 0.05$), from 49.6 to 55.2. After 1 hour of

hyperbaric oxygen recovery, there was a significant decrease compared with before the hyperbaric oxygen recovery ($p < 0.05$), dropped from 55.2 to 53.1. It illustrates the success of the experiment results after the ferroelectric material is used in sports scientific research. It also completed the subject of interaction and combination of the performance and modification of bismuth-layered ferroelectric materials in sports scientific research. The shortcomings of this article are as follows: (1) use long-distance running as the basis of the subject for research and does not consider sports such as long jump and various ball sports. In future research, the research content can be gradually improved and expanded to more sports items. (2) Among the research materials in this article, due to the limitation of experimental site and funding, only the research on $Bi_4Ti_3O_{12}$, a layered bismuth ferroelectric material, has been carried out. In future research, efforts can be made to find bismuth-layered ferroelectric materials with cheaper prices, better experimental results, and ferroelectric properties more in line with experimental requirements. (3) Due to time and space constraints, this article only conducted a 4-week training for the two groups to collect heart rate indicators. In future research, the experimental time and interval length can be extended to ensure the scientific reliability of the experimental results.

Data Availability

No data were used to support this study.

Conflicts of Interest

There is no potential conflict of interest in this study.

References

[1] M. A. Basheer, G. Prasad, G. S. Kumar, and N. V. Prasad, "Raman and electrical studies on $Bi_2SmTiNbO_9$ ceramics," *Ferroelectrics*, vol. 517, no. 1, pp. 75–80, 2017.

[2] R. Nie, J. Yuan, and J. Zhu, "Influence of co-modification with tungsten and tantalum on the crystal structure and electrical properties of bismuth titanate ceramics," *Journal of Materials Science Materials in Electronics*, vol. 30, no. 15, pp. 14445–14455, 2019.

[3] P. Ketwong, P. Kidkhunthod, and P. Pookmanee, "Effect of ethanol assistance on chemical structure of ferroelectric bismuth vanadate via solvothermal method," *Integrated Ferroelectrics*, vol. 175, no. 1, pp. 9–17, 2016.

[4] Z. Liu, A. R. Paterson, H. Wu, P. Gao, W. Ren, and Z. G. Ye, "Synthesis, structure and piezo-/ferroelectric properties of a novel bismuth-containing ternary complex perovskite solid solution," *Journal of Materials Chemistry C*, vol. 5, no. 16, pp. 3916–3923, 2017.

[5] E. V. Ramana, N. V. Prasad, D. M. Tobaldi et al., "Effect of samarium and vanadium co-doping on structure, ferroelectric and photocatalytic properties of bismuth titanate," *RSC Advances*, vol. 7, no. 16, pp. 9680–9692, 2017.

[6] T. Obayashi, M. Kobune, T. Matsunaga et al., "Effects of Pt sacrificial layer on microfabrication in layered bismuth-based ferroelectric thin films," *Transactions of the Materials Research Society of Japan*, vol. 45, no. 2, pp. 31–34, 2020.

[7] H. Maleki, "Photocatalytic activity, optical and ferroelectric properties of $Bi_{0.8}Nd_{0.2}FeO_3$ nanoparticles synthesized by sol-gel and hydrothermal methods," *Journal of Magnetism& Magnetic Materials*, vol. 458, no. 1, pp. 277–284, 2018.

[8] S. N. Das, S. Pradhan, S. Bhuyan, R. N. Choudhary, and P. Das, "Modification of relaxor and impedance spectroscopy properties of lead magnesium niobate by bismuth ferrite," *Journal of Electronic Materials*, vol. 46, no. 3, pp. 1637–1649, 2017.

[9] Y. Zhang, M. Yuan, B. Jiang, P. Li, and X. Zheng, "Effect of mesoporous structure on $Bi_{3.25}La_{0.75}Ti_3O_{12}$ powder for humidity sensing properties," *Sensors& Actuators B Chemical*, vol. 229, no. 2, pp. 453–460, 2016.

[10] X. Chen, F. Huang, Z. Lu et al., "Influence of transition metal doping (X=Mn, Fe, Co, Ni) on the structure and bandgap of ferroelectric $Bi_{3.15}Nd_{0.85}Ti_2X_1O_{12}$," *American Political Science Review*, vol. 54, no. 2, pp. 948–979, 2017.

[11] X. Chen, F. Huang, Z. Lu et al., "Influence of transition metal doping (X=Mn, Fe, Co, Ni) on the structure and bandgap of ferroelectric $Bi_{3.15}Nd_{0.85}Ti_2X_1O_{12}$," *Journal of Physics: D Applied Physics*, vol. 50, no. 10, article 105104, 2017.

[12] M. Hasan, M. A. Hakim, M. A. Basith et al., "Size dependent magnetic and electrical properties of Ba-doped nanocrystalline $BiFeO_3$," *AIP Advances*, vol. 6, no. 3, pp. 2–8, 2016.

[13] G. Hernandez-Cuevas, J. R. Leyva Mendoza, P. E. García-Casillas et al., "Effect of the sintering technique on the ferroelectric and d_{33} piezoelectric coefficients of $Bi_{0.5}(Na_{0.84}K_{0.16})_{0.5}TiO_3$ ceramic," *Journal of Advanced Ceramics*, vol. 8, no. 2, pp. 278–288, 2019.

[14] E. D. Politova, G. M. Kaleva, N. V. Golubko et al., "Specific features of the structure and properties of high-temperature oxide materials based on bismuth sodium titanate," *Crystallography Reports*, vol. 63, no. 2, pp. 266–270, 2018.

[15] L. X. Chen, C. Xu, X. L. Fan, X. H. Cao, K. Ji, and C. H. Yang, "Study on leakage current, ferroelectric and dielectric properties of BFMO thin films with different bismuth contents," *Journal of Materials Science: Materials in Electronics*, vol. 30, no. 8, pp. 1–7, 2019.

[16] I. Soibam and M. A. Devadatta, "Optimisation and the effect of addition of extra bismuth on the dielectric and optical properties of bismuth ferrite (BFO)," *Materials Today Proceedings*, vol. 5, no. 1, pp. 2064–2073, 2018.

[17] R. A. Golda, A. Marikani, and E. J. Alex, "Effect of ceramic fillers on the dielectric, ferroelectric and magnetic properties of polymer nanocomposites for flexible electronics," *Journal of Electronic Materials*, vol. 50, no. 6, pp. 3652–3667, 2021.

[18] L. Thansanga, A. Shukla, N. Kumar, and R. N. Choudhary, "Study of effect of Dy substitution on structural, dielectric, impedance and magnetic properties of bismuth ferrite," *Journal of Materials Science: Materials in Electronics*, vol. 31, no. 13, pp. 10006–10017, 2020.

[19] A. Panda, R. Govindaraj, R. Mythili, and G. Amarendra, "Formation of bismuth iron oxide based core–shell structures and their dielectric, ferroelectric and magnetic properties," *Journal of Materials Chemistry C*, vol. 7, no. 5, pp. 1280–1291, 2019.

[20] C. Aydin, H. Aydin, M. Taskin, and F. Yakuphanoglu, "A novel study: the effect of graphene oxide on the morphology, crystal structure, optical and electrical properties of lanthanum ferrite based nano electroceramics synthesized by hydrothermal

method," *Journal of Nanoscience and Nanotechnology*, vol. 19, no. 5, pp. 2547–2555, 2019.

[21] N. A. Zhuk, S. V. Nekipelov, D. S. Beznosikov, L. V. Rychkova, M. V. Yermolina, and B. A. Makeev, "Magnetic properties and NEXAFS-spectroscopy of Co-doped ferroelectric ceramic $Bi_5Nb_3O_{15}$," *Letters on Materials*, vol. 9, no. 4, pp. 405–408, 2019.

[22] D. Ruth, L. Venkidu, and B. Sundarakannan, "Structure–property relation to enhance the piezoelectric and ferroelectric properties in $(Na_{0.5}Bi_{0.5})$ TiO_3-based non-MPB lead-free piezoelectric ceramics," *Journal of Materials Science: Materials in Electronics*, vol. 29, no. 7, pp. 5433–5438, 2018.

[23] S. Chakraborty, S. Mukherjee, and S. Mukherjee, "Effect of yttrium doping on the properties of bismuth ferrite: a review," *International Journal of Semiconductor Science& Technology*, vol. 8, no. 2, pp. 23–32, 2018.

[24] G. Parida and J. Bera, "Effects of CuO additive on ferroelectric and dielectric properties of Nb doped $SrBi_8Ti_7O_{27}$ ceramics," *Journal of Materials Science Materials in Electronics*, vol. 27, no. 5, pp. 5309–5314, 2016.

[25] A. Klr, B. Ds, and A. Db, "Gamma irradiation induced structural, electrical, magnetic and ferroelectric transformation in bismuth doped nanosized cobalt ferrite for various applications," *Materials Research Bulletin*, vol. 110, no. 10, pp. 126–134, 2019.